Hyperspectral imaging of atherosclerotic plaques *in vitro*

Eivind L. P. Larsen,ᵃ Lise L. Randeberg,ᵃ Elisabeth Olstad,ᵇ Olav A. Haugen,ᶜ Astrid Aksnes,ᵃ and Lars O. Svaasandᵃ

ᵃNorwegian University of Science and Technology, Department of Electronics and Telecommunications, 7034 Trondheim, Norway
ᵇUniversity Hospital of North Norway, Department of Radiology, Division of Diagnostic Services, 9038 Tromsø, Norway
ᶜChildren's and Women's Health, Norwegian University of Science and Technology, Department of Laboratory Medicine, 7006 Trondheim, Norway

Abstract. Vulnerable plaques constitute a risk for serious heart problems, and are difficult to identify using existing methods. Hyperspectral imaging combines spectral- and spatial information, providing new possibilities for precise optical characterization of atherosclerotic lesions. Hyperspectral data were collected from excised aorta samples ($n = 11$) using both white-light and ultraviolet illumination. Single lesions ($n = 42$) were chosen for further investigation, and classified according to histological findings. The corresponding hyperspectral images were characterized using statistical image analysis tools (minimum noise fraction, K-means clustering, principal component analysis) and evaluation of reflectance/fluorescence spectra. Image analysis combined with histology revealed the complexity and heterogeneity of aortic plaques. Plaque features such as lipids and calcifications could be identified from the hyperspectral images. Most of the advanced lesions had a central region surrounded by an outer rim or shoulder-region of the plaque, which is considered a weak spot in vulnerable lesions. These features could be identified in both the white-light and fluorescence data. Hyperspectral imaging was shown to be a promising tool for detection and characterization of advanced atherosclerotic plaques *in vitro*. Hyperspectral imaging provides more diagnostic information about the heterogeneity of the lesions than conventional single point spectroscopic measurements. © *2011 Society of Photo-Optical Instrumentation Engineers (SPIE)*. [DOI: 10.1117/1.3540657]

Keywords: hyperspectral imaging; atherosclerosis; optical diagnostics.

Paper 10211PRR received Apr. 21, 2010; revised manuscript received Dec. 21, 2010; accepted for publication Dec. 21, 2010; published online Feb. 22, 2011.

1 Introduction

The formation of plaques in arteries, atherosclerosis, is a slowly progressing condition which constitutes the pathological basis for common diseases such as heart attacks and strokes. Atherosclerosis with associated complications is a major contributor to morbidity and mortality in the world today.[1] In a clinical setting there is a need to diagnose atherosclerosis to determine the right time for intervention, choice of treatment, and assessment of prognosis.

This is a complex task which requires thorough knowledge about the properties of both the lesion and the adjacent vessel wall. The current gold-standard in clinical use for examination of coronary arteries is angiography, however, it is limited to detecting only stenotic plaques. A large effort has been put into characterization of atherosclerotic plaques and developing new diagnostic tools. The use of optical techniques for this purpose has thus been extensively explored in the past, by, e.g., spectroscopic techniques such as diffuse- and near-infrared reflectance spectroscopy,[2–4] laser-induced fluorescence spectroscopy,[4–8] and imaging modalities such as optical coherence tomography[9,10] and angioscopy.[11,12] Other fluorescence properties of tissue are also employed in advanced microscopy techniques such as FLIM (fluorescence lifetime imaging mi-

croscopy) and multiphoton microscopy, which have also been used to identify atherosclerotic lesions *in vitro*.[13,14] These techniques have been proven useful in previous work, but so far the clinical implementation of the different modalities have had limited success.

Hyperspectral imaging (HSI) is a relatively new tool in medicine. This technique brings optical characterization one step further by providing high spectral and spatial resolution in one measurement. This combination allows for spectral analysis of each pixel in the acquired image, and also facilitates advanced statistical image analysis of the entire image. In recent years, HSI has proved to be a useful modality in diagnostic medicine including applications for retinal imaging,[15,16] skin diagnostics,[17–20] and tumor microvasculature mapping and cancer detection.[21–24]

Fluorescence light detection has been used in some HSI-systems,[13,25,26] and also in combination with reflectance imaging.[27] The combination of both white-light HSI and laser-induced fluorescence HSI has the potential of revealing more information about the material under investigation. This makes it possible not only to detect atherosclerotic plaques, but also to find characteristics of different plaque types.

This study presents hyperspectral reflectance and fluorescence data of atherosclerotic lesions from human aortic samples, with focus on advanced lesions. The main goal of this paper is

Address all correspondence to: Lise L. Randeberg, University Hospital of North Norway, Department of Radiology, Division of Diagnostic Services, 9038 Tromsø, Norway; E-mail: lise.randeberg@iet.ntnu.no.
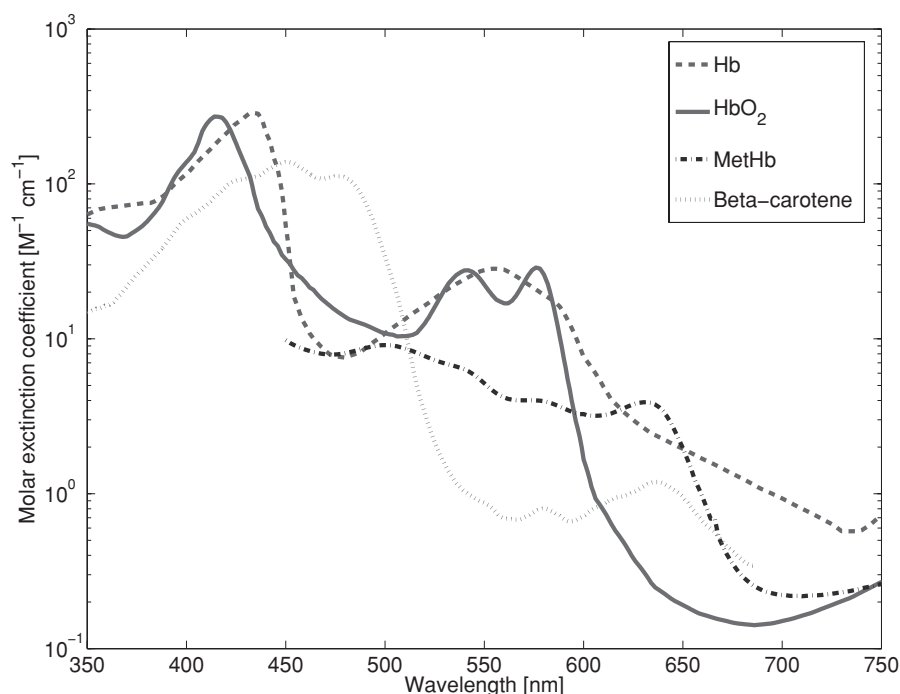
Fig. 1 Molar extinction coefficients of oxygenated and deoxygenated hemoglobin (Ref. 33), methemoglobin (Ref. 34), and beta-carotene (Ref. 37).

to give a comparative overview of white light and fluorescence properties of the investigated samples, with a special focus on spatial variation. Characterization of lesions was performed according to spectral features using image analysis combined with histology. Aortic samples are used in this work as they are convenient to study due to their size. The presented information can hopefully be used as a basis for development of simpler, more clinically relevant systems.

2 Background

2.1 Atherosclerosis

In atherosclerosis, deposits forming atheromatous plaques develop in the artery wall, and these plaques can be more or less vulnerable to rupture constituting a risk for the patient.[28–31] To correctly determine the diagnosis, prognosis, and the required treatment of advanced atherosclerosis, a modality capable of differentiating vulnerable plaques from stable plaques is required. However, the definition of a vulnerable plaque is a functional one and not based on anatomic appearance. Studies have indicated some common features of plaque vulnerability, such as a thin fibrous cap, a large lipid content, the presence of haemorrhagic areas, and degree of inflammation.[28] During the process of plaque formation, different stages can be identified, and this forms the basis for the current classification systems. A frequently used system was proposed by the American Heart Association (AHA),[30,31] and is based on histological examination of arteries from autopsies. Plaques are divided into early lesions (grade I-II), intermediate lesions (grade III), and advanced lesions (grade IV-VI). The use of roman numerals indicates a successive development through all stages which is not necessarily the case, as pointed out

by Virmani et al., who have proposed changes to the AHA-classification.[32]

2.2 Optical Properties

To detect and characterize atherosclerotic plaques it is necessary to identify the various chromophores and fluorophores of both healthy and pathologic tissue.

The most important chromophores in this application are different forms of hemoglobin, lipids/ carotenoids, connective tissues (collagen and elastin), and calcifications. Hemoglobin is a pronounced absorber with characteristic absorption spectra according to the oxygenation of the molecule, see Fig. 1. Deoxygenated hemoglobin has absorption maxima at 433, 554, and 760 nm, and appears dark red with a bluish tint. Oxygenated hemoglobin has absorption maxima at 414, 542, and 576 nm,[33] and appears bright red. Methemoglobin is a defect hemoglobin molecule (caused by oxidative stress) with no oxygen carrying capability, and appears dark brown with absorption peaks at 404, 508, and 635 nm (see Fig. 1).[34,35]

Lipid rich plaques have a higher concentration of carotenoids, mainly betacarotene, than normal aortic tissue.[36] Beta-carotene has two characteristic absorption peaks at 450 and 480 nm,[37,38] (see Fig. 1), and accumulates in fatty tissue causing the yellow color of such tissue. Beta-carotene is therefore an indicator of lipids. Likewise, superficial foam cells, which may be an indicator of plaque vulnerability, have been shown to have beta-carotene absorption, as such foam cells may contain lipids.[4] Water absorption is low in the visible region, but has absorption peaks in the NIR and IR regions. The absorption peak at 980 nm can be detected with the camera setup used in this work. Scattering from biological tissue is a combination of Mie- and Rayleigh

scattering, and generally falls off monotonously with increasing wavelength.[39] In soft tissues, scattering is most pronounced for shorter wavelengths where it is dominated by small fibrils such as collagen.

The major fluorophores expected to be present in normal aortic tissue and atherosclerotic plaques are collagen, elastin, and carotenoids.[7,40] If multiple fluorophores are present, the pure spectra of each fluorophore are superpositioned, and if other absorbers are present the fluorescence spectra will be affected accordingly. Collagen is known to exhibit strong autofluorescence at approximately 450 nm.[41]

3 Materials and Methods

3.1 Aortic Samples

Measurements were performed on sections from the aorta excised during autopsies. A total of 11 samples were obtained from males 65 to 85 years old, eight of the eleven subjects died from complications associated with the circulatory system/ cardiovascular diseases. Acquisition of the hyperspectral images were performed 1 to 4 days *post mortem*. The samples had various degrees of atherosclerosis. After excision, the aorta sections were opened longitudinally to provide samples of size approximately 6×8 cm. They were then rinsed with saline to remove superficial blood, wrapped in a moist towel (saline) and kept cool for storage, transport, and in between measurements. The samples were placed on a piece of black, nonfluorescent plastic to ensure even illumination and avoid (fluorescent) light originating from the background. Fluorescence images were obtained after white-light images had been recorded. Hyperspectral data from the lumen was recorded with a HSI-system using a white-light lamp and a UV-laser for illumination.

The project was approved by the Regional Committee for Medical and Health Research Ethics, Norway.

3.2 Hyperspectral Camera Setup

The imaging system was based on a HySpex VNIR-1600 (Norsk Elektrooptikk AS, Oslo, Norway) push-broom hyperspectral camera. The camera utilizes a polarization independent grating and a Si-CCD detector (1600 spatial pixels) which yields 160 bands in the 410 to 1000-nm wavelength region (3.7-nm separation).[42] The camera records one line at a time, hence scanning along one axis is necessary to construct a 2D-imag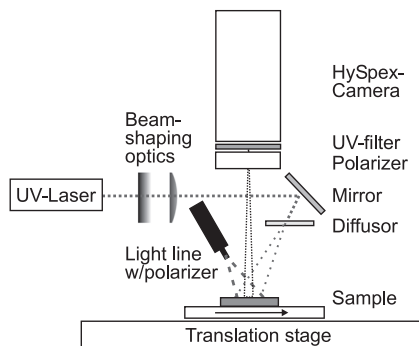e. The camera was mounted on a rack facing downward (birds-eye view). The samples were placed on a table mounted on a translation stage, see Fig. 2. A 150W dc white-light source with a 12.5-cm wide fiber optic line light guide (DCR II, Fostec, Auburn, New York) provided illumination of the sample. Specular reflections dramatically deteriorate image quality as the reflected light affects the measured spectrum and/or saturates the detector, masking the true reflection spectrum of the sample. The light source was set at an angle that minimized the specular reflections from the sample surface. Furthermore, as the samples are not flat, a linear polarizer film (International Polarizer Inc, Marlboro, Massachusetts) was fitted to the light line, and a second polarizer (NT52-574, Edmund Optics, York, UK) was placed in front of the camera lens and rotated to minimize specular reflections. This effectively suppressed spectral reflections, but due to limited bandwidth of the polarizers this was only effective up to 750 nm. As a consequence, all spectra were truncated to 410 to 750 nm (95 bands) for analysis.

For fluorescence imaging a pulsed, frequency tripled Nd:YAG-laser (Quanta Ray Lab-series L-190, Spectra Physics, Mountain View, California) provides UV-excitation (355 nm) of the sample. The laser output was shaped to a line using two cylindrical lenses (plano-concave and plano-convex, Newport Corp., Irvine, California) and projected by a mirror via a diffusor onto the sample, as presented in Fig. 2. The diffuser broadens the line to ensure uniform excitation light distribution over the camera's field of view as the samples were not perfectly flat. The irradiance on the sample was approximately 20 to 30 mW/cm^2.

In Fig. 3 the concept of a hyperspectral imaging cube is shown, where two spatial axes (x, y) represent the 2D-image, and the z-axis represents the spectral information (amplitude) at different wavelength bands.

3.3 Image Acquisition

The samples were scanned along the x-axis to construct a 2D-hyperspectral image. A full scan takes approximately 30 s to complete, depending on the scan settings such as scan (translation) length, exposure time, and averaging.

For white-light reflectance measurements an optical reflection standard (Spectralon WS-1, Ocean Optics, Duiven, The
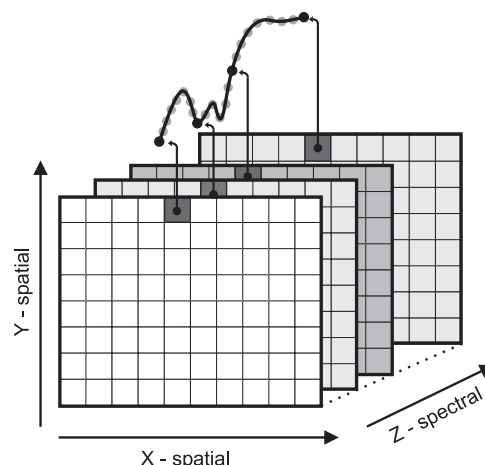

Fig. 2 Measurement setup.

Fig. 3 Hyperspectral imaging principle.

Netherlands) was placed beside the sample and recorded in the image. The reflection standard allows for calibration of the raw radiance image versus the illumination lamp spectrum to yield the true reflectance image. A radiometric calibration was performed automatically by the camera software to compensate for the detector response and dark current noise, producing true radiance images.

Fluorescence images were obtained directly after visible images had been recorded. The camera polarizer was removed before fluorescence measurements to improve the signal-to-noise ratio as the polarizer attenuates the light. The positioning of the sample and spatial scan settings were maintained during both measurements to have co-registered reflectance and fluorescence-images.

A preliminary analysis of the hyperspectral images was performed directly after the images were acquired, and three to six areas of interest were identified on each sample. The selection of these sites was based on both macroscopic determination of plaques and lesions, and also on areas with abnormal spectra found in the preliminary analysis. Plaques assumed to be advanced lesions were preferred in the selection. These areas of interest were later excised for further histological examination. In total there were 42 biopsies from the eleven samples.

3.4 Histological Examination and Lesion Classification

The areas of interest were excised for biopsies (10×8 mm), bisected, and inkmarked; one-half was snap-frozen in liquid nitrogen and the other half fixed in 10% buffered formalin and later embedded in paraffin. The biopsies were then sliced and stained, the frozen halves with Oil red O and the paraffin embedded with hematoxylin-eosin-saffron (HES), Van Gieson, Gordon/Sweet and elastin stains.

The stained sections from the aorta samples were examined using a standard light microscope at three magnifications (ob. 5×, 10×, and 20×), and photographed. The three layers of the arterial wall (intima, media, and adventitia) were identified and the thickness of the intima was measured and defined as the distance from the media to the lumen surface. Lesions and plaques were classified according to the AHA-classification scheme as type I-VI.[30, 31] Of the advanced lesions, IV and Va are lipid laden lesions considered the most vulnerable plaque types. Type Vb represent calcified lesions, and type Vc are fibrotic lesions without calcifications or a lipid core. Type VI-lesions are ulcerated (ruptured) plaques. The classification was based on plaque features such as the presence of calcium deposits, foam cells, lipid core, cholesterol clefts, macrophage infiltration, fibrous cap, media influence, and the size of these features such as cap thickness and total plaque thickness, when present. The size was found by using a ruler calibrated to an image of a microscope measurement gauge taken at the same magnification. If there was a large discrepancy of the thickness of these features across the length of the section, both the minimum and the maximum thickness were measured.

3.5 Data Analysis

The hyperspectral camera records 160 continuous bands in the 400 to 1000 nm range for each image element, and consequently generates a large amount of data in need of further processing and analysis (approx. 1 Gb per image). Commercially available software was used for the analysis of the acquired images, Environment for Visualizing Images (ENVI and IDL, ITT Visual Information Solutions, Bracknell, Berkshire, UK). The HySpex acquisition software exports images to a standard format read by ENVI. Raw image data were converted to reflectance data in ENVI by performing a flat field calibration routine in reference to the Spectralon-tile.

3.5.1 Image analysis methodology

Several image analysis tools were used to classify the pixels of the hyperspectral images, and hence the components of the recorded object. Due to the many wavelength bands in hyperspectral imagery, much of the data collected is highly correlated and therefore redundant. To reduce spectral redundancy and emphasize the importance of unique spectral features, the spectral datasets can be transformed. Transformations decorrelate and compact spectral information into fewer bands with decreasing coherence, i.e., only the first band in the transformed image will contain interesting information, simplifying further analysis.

The minimum noise fraction transform (MNF) implemented in ENVI was used to reduce the spectral dimensionality and noise in the hyperspectral images. The MNF transform is a linear transformation which is essentially two cascaded principal components analysis (PCA) transformations. The transform reduces the dimensionality of the data space by separating noise from the image data.[43] The first transformation decorrelates and rescales the noise in the data. This results in transformed data in which the noise has unit variance and no band to band correlations. The second transformation is a standard PCA of the noise-whitened data, effectively yielding two data sets; one part with large eigenvalues corresponding to coherent image data, and a complementary part with near-unity eigenvalues associated with incoherent noise which can be discarded.[43] The number of MNF-bands is substantially less compared to the original hyperspectral image, typically 3 to 10 MNF-bands versus 95 original bands. MNF is also referred to as noise whitened PCA.

A variety of segmentation and classification techniques can be employed in further analysis of hyperspectral datasets. In this work classification of the MNF-transformed images was performed by using the *K*-means classification routine. *K*-means classification is an unsupervised classification technique which aims to sort the image pixels into *k*-groups based on image statistics. The algorithm first calculates class means for a predefined number of classes (*k*) evenly distributed over the data space. The image pixels are then distributed into the class which have (spectral) means closest to the pixel spectral signature. The algorithm then recalculates the means and reclassifies the pixels iteratively until the number convergence is achieved, or the maximum number of allowed iterations is reached.[44] The 42 areas of interest subject for histological examination were also the focus for further hyperspectral image analysis. A region of 400×400 pixels (approx 2×2 cm) was defined around each area, and these smaller regions were investigated by image analysis techniques. Each region was MNF transformed to remove noise, and images were averaged over 5×5 pixels prior to *K*-means classification to avoid classification of single pixels. The resulting classification map was then projected onto the original hyperspectral

(a)

(b)
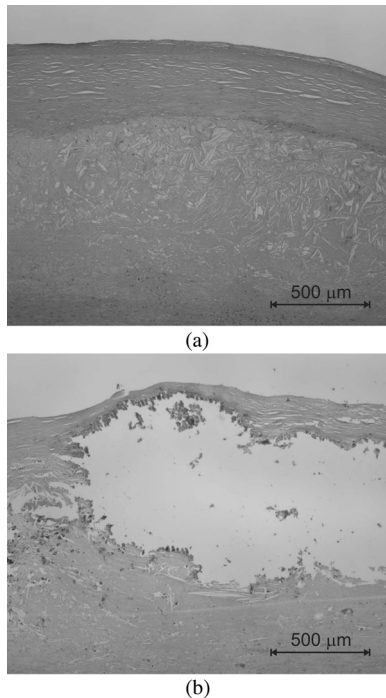
Fig. 4 (a) Photomicrographs of a grade Va-plaque and (b) a grade Vb-plaque classified according to the AHA-classification.

(a)

(b)

Fig. 5 (a) Pseudo-RGB images of an aortic sample; white-light reflectance image and (b) UV-excitation autofluorescence image.

image, and the regions corresponding to the biopsy sites used for histological classification were identified. The mean spectra of these regions were collected for all 42 samples. This allowed for direct comparison of the plaque spectra, and was performed on both the reflectance- and fluorescence hyperspectral image data.
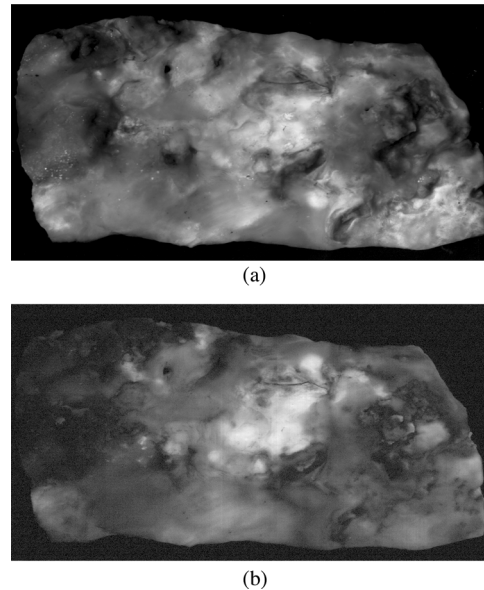
3.5.2 PCA and statistical analysis

The mean reflectance- and fluorescence spectra collected from the 42 plaques based on *K*-means classification were analyzed using PCA in Matlab (Matlab 2008b, The MathWorks AB, Kista, Sweden). The PCA analysis was based on the histological classification of the samples, and the PCA results were examined in this context. All areas of interest were included in the analysis. Statistical analysis was performed using the statistics toolbox in Matlab.

4 Results

4.1 Macroscopic Evaluation of Aorta Samples

The aorta tissue samples were examined macroscopically. A photograph of a representative sample is shown in Fig. 5(a). Areas of apparently normal vessel wall, as well as areas with macroscopically visible atheromatous changes, were present in all samples. The normal vessel wall had a gross appearance with smooth, pale yellow colored lining and a soft texture, whereas areas with atherosclerotic plaques demonstrated elevation of the vessel lining and had a darker yellow, red or brown color. Furthermore, the intimal surface was irregular and partially ruptured or ulcerated and the texture was firm or even hard. The plaques were of different sizes and varied in shape from round to oval or irregular. Particularly in the larger and most severe atheroscle-

rotic areas, the appearance of one single plaque could differ considerably between different regions of the plaque, and some lesions seemed to have merged by the expansion of adjacent plaques.

4.2 Microscopic Evaluation of Aorta Tissue Samples

The atherosclerotic plaques were evident as areas of the intima with increased thickness ($215 \pm 167 \ \mu$m), whereas in the biopsies without evident plaques ($n = 4$), the intima thickness was $120 \pm 25 \ \mu$m. It is important to notice that areas of the arterial wall without plaques also show some degree of morphological changes such as increased intima thickness, increased amount of collagen fibers in the intima, and decreased amount of elastin fibers in the media. These changes are normal with age (subjects age 72.3 ± 6.5 years, range 64 to 85), and these samples can be considered age matched controls. Most of the plaques had a cap consisting of collagen rich fibrous tissue overlying a necrotic center mainly containing lipids, partly in the form of cholesterol clefts and foam cells. In some samples, nodules of calcium were present in the center of the plaque, and in others larger areas of calcification were evident [calcified areas are usually traumatized during the section preparation, and appear as "empty" areas with surrounding remains of dark purple stained tissue as seen in Fig. 4(b)].

The plaques demonstrated a various amount of foam cells characterized by the presence of vacuoles (containing lipid) in the cytoplasm. The foam cells were, in many instances, located at the peripheral regions, the shoulder, of the plaque. However, in some cases a considerable number of foam cells were seen in the cap.

The intima thickness was measured in each sample as the distance from the lumen to the media defined as the presence of elastin fibers visible as the eosinic base-layer in Figs. 4(a) and 4(b).
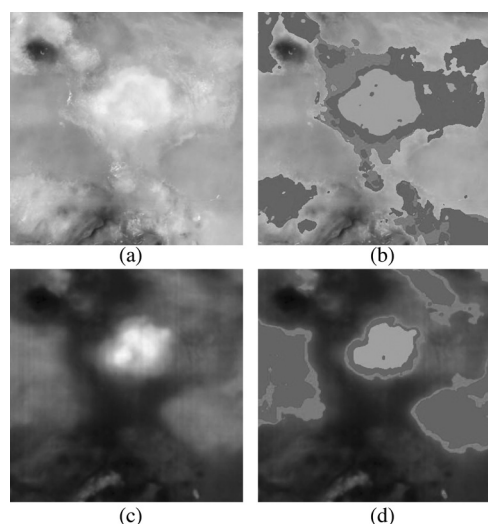
Fig. 6 (a) White-light reflectance image and UV-excited autofluorescence image (c) of an advanced plaque. The corresponding K-means classification overlays are shown in (b) (white-light) and (d) (fluorescence).

4.3 *Frequency of Population Lesion Types Based on Histology*

The majority of plaques were found to be advanced lesions; 38 of the 42 areas of interest were classified as grade IV and Va (20), Vb (11), Vc (5), and VI (2) lesions. The remaining lesions consisted of three grade I- and one grade II lesion. No completely healthy aortic wall tissue (grade 0) were among the sampled biopsies, as even the most healthy regions showed intimal thickening (grade I-II), not to be unexpected in the elderly demographic. No grade III lesions were found.

4.4 *Lesion Characterization Based on Hyperspectral Image Analysis*

Figure 5(a) shows a pseudo-RGB image of a tissue sample (from 77 y.o. male) as acquired by the HySpex-camera under white-light illumination (bands $R = 608$ nm, $G = 557$ nm, and $B = 451$ nm, all RGB-images presented use these bands). Figure 5(b) shows the same tissue sample acquired under UV-excitation. As these images clearly demonstrate, there are various regions which can easily be distinguished by the naked eye based on their visual appearance. Note how the leftmost region of the sample appears red under white-light illumination in Fig. 5(a), and almost completely dark under UV-excitation as shown in Fig. 5(b), while the central region appears white and bright white correspondingly. More subtle differences can be found by examining the corresponding wavelength spectra of the hyperspectral image pixels, and allows for differentiating and possibly classifying the various regions of the samples accordingly. Figure 6 shows an advanced plaque (type Vb, from 85 y.o. male) under white-light illumination, Fig. 6(a), and the UV-excitation autofluorescence image of the same plaque in Fig. 6(c). The corresponding K-means classification images are shown in Figs. 6(b) and 6(d) based on the reflection- and fluorescence image, respectively. Note how in both classification images there is a central region surrounded by one or more regions of different spectral characteristics determined by the K-means classification, suggesting a


(a)

(b)
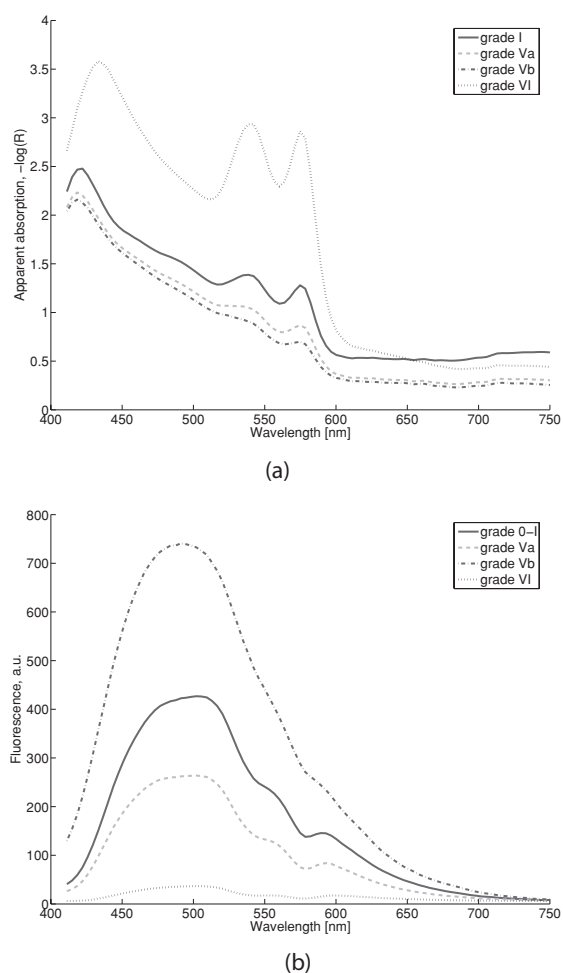
Fig. 7 (a) Apparent absorption spectra and (b) fluorescence spectra (not normalized) of grade I, Va, Vb and VI-plaques from the same aorta sample.

heterogeneous plaque. Figure 7 shows spectra from regions of the same aorta sample, however, these regions were histologically classified as different grade lesions. The spectra in Fig. 7(a) shows the apparent absorption spectra [-log(Reflectance)] of grade I, Va, Vb, and VI plaques and Fig. 7(b) show the corresponding fluorescence spectra. The spectra of the grade VI plaque differs significantly from the others as it has a much higher apparent absorption, and also expresses low fluorescence as compared to the other grade lesions. Note also that the largest absorption peak has redshifted to 433 nm as compared to 418 nm for the other spectra. The other absorption spectra appear more homogeneous, and a small local maximum can be observed around 480 nm. The fluorescence spectra however, differ significantly. The Vb-grade (calcified) plaque exhibits a very strong fluorescent signal compared to the others.

4.4.1 *Reflectance and fluorescence images*

Figure 8 shows a HES-stained histological section of a grade Va-lesion. The plaque is the thickened, lighter part (p) on top of the darker (eosin) stained media (m). The arrow on the left indicates a shoulder-region of the plaque with foam cells and
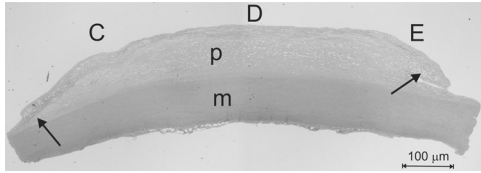
Fig. 8 Histological section of grade Va-plaque, letters corresponding to positions as indicated in Figs. 9 and 10.

cholesterol crystallization with early stages of calcification. There are visible dense collagen fibers in the cap layer. As one moves rightward along the plaque (C and D) these collagen fibers become more separated in regions where other necrotic materials are entwined between these fibers. The underlying core (D) contains foam cells and evidence of cholesterol and necrotic material. Toward the other end of the section (E), foam cells are evident near the surface and at the shoulder (arrow to the right). Figures 9 and 10 show reflectance and fluorescence images of the same HES-stained plaque shown in Fig. 8 (from 74 y.o. male). The spectra [Figs. 9(b) and 10(b)] are harvested from sites along a straight line (indicated by letters A, B, C, D, and E), also corresponding to the direction of the cut for the histology section (Fig. 8). The letters C, D, and E along the section in Fig. 8 correspond to positions in the hyperspectral reflectance and fluorescence images shown in Figs. 9 and 10.

Site A from the hyperspectral reflectance image in Fig. 9 is from a lesion free area of the aorta. The corresponding apparent absorption spectrum shows no distinct features other than absorption peaks in the 540 to 580 nm range, plus the slightly redshifted absorption peak in the Soret-band. Site B appears lighter than site A, and the corresponding spectrum demonstrates lower absorption, and a small local maximum can be observed around 480 nm. Site C appears even lighter and is, as established from Fig. 8, a region of the plaque with separated collagen fibers over foam cells. The apparent absorption spectrum shows lower absorption than site B, and the spectrum is quite similar to the spectrum of site D which is from a part of the plaque with a thicker lipid core. The spectrum of site E shows a large absorption in the 450 to 490 nm region.

Figure 10 shows the co-registered hyperspectral fluorescence image of the same sample. The normal tissue (site A) exhibits a pronounced fluorescence with a main peak around 510 nm, and the right (red) side fluorescence tail quenched in the 540 to 580 nm region corresponding to hemoglobin absorption. Sites B and C fluorescence spectra are quite similar in shape and had the overall lowest fluorescence of the sites. A local minimum centered around 480 nm is visible. Site D has the highest overall fluorescence with a maximum around 450 nm, and a small crease around 480 nm. Site E has a main peak above 500 nm and the spectra also display a substantial re-absorption of light around 480 nm.

Generally, autofluorescence could be detected from the entire surface of the samples, also from the regions classified as normal by histology. Calcified regions show the strongest overall fluorescence centered around 470–500 nm; the absorption effect of hemoglobin and beta-carotene could be readily seen near the circumference of calcified regions in the spectra, but to a lesser degree in the center of calcified regions. The lowest
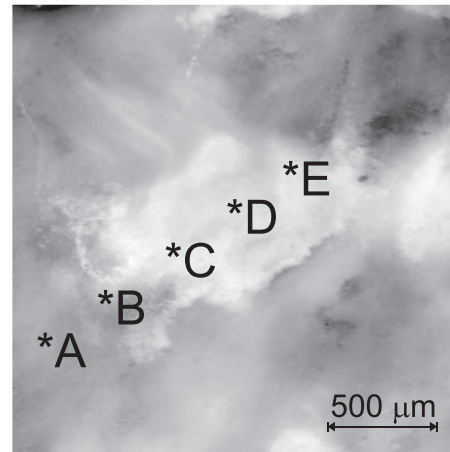

(a)
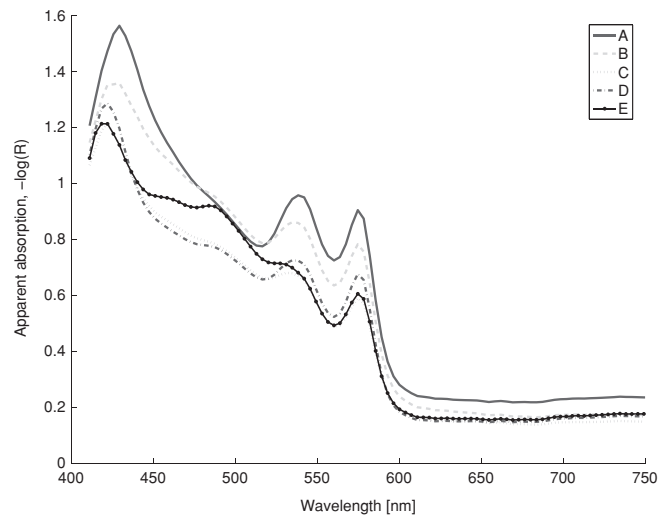
(b)

Fig. 9 (a) Atherosclerotic plaque under white-light illumination and (b) corresponding spectra.

overall autofluorescence levels were observed in regions with high hemoglobin and beta-carotene absorption, classified as grade VI.

4.4.2 *PCA and statistical analysis*

For reflectance data, the first and most significant PCA eigenvector reveal maxima/ minima at 420, 515, 537, 558, and 573 nm. The second PCA eigenvector has extrema at 432, 486, 541, 557, and 574 nm. The third eigenvector has maxima/ minima at 415, 464, and 603 nm. PCA of the corresponding fluorescence data revealed maxima/minima at 482, 577, and 596 nm for the most significant eigenvector; 433, 511, 541, 555, 573, and 599 nm for the second eigenvector; and 482, 537, 559, 573, and 610 nm for the third eigenvector. Based on analysis of the cumulative variance for the PCA components, it was found that the first three PCA components were significant. Analysis of the reflectance- and fluorescence spectra as two separate batches revealed only slight differences between the histology groups, although the groups were found to be robust with regard to the contribution from the individual samples (leave-one-out or
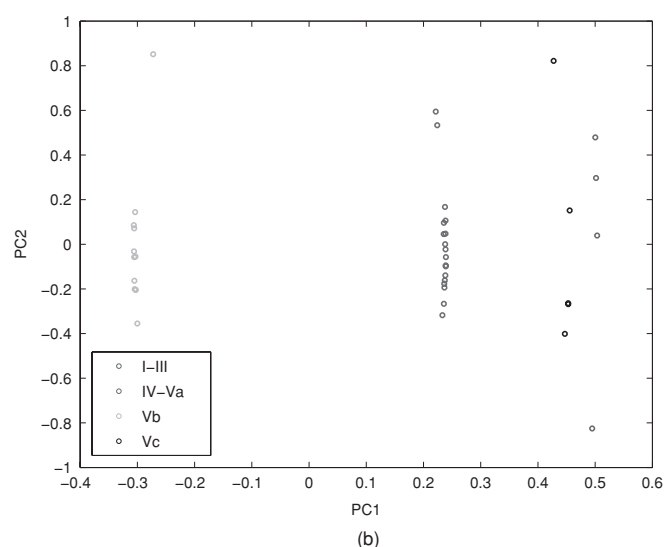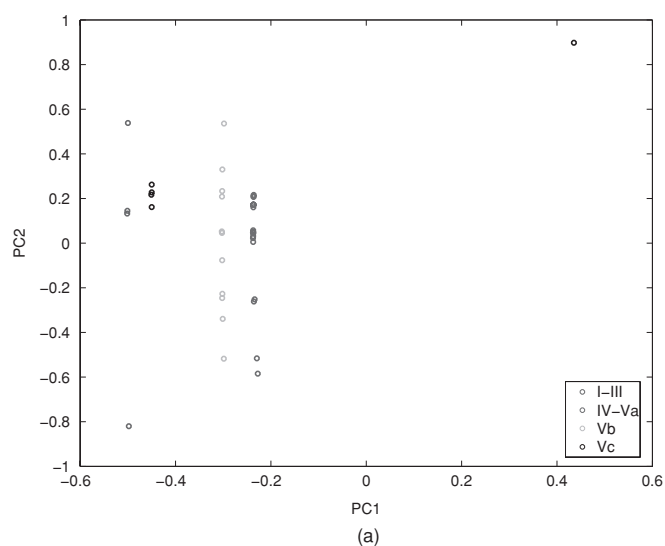
(a)

(b)
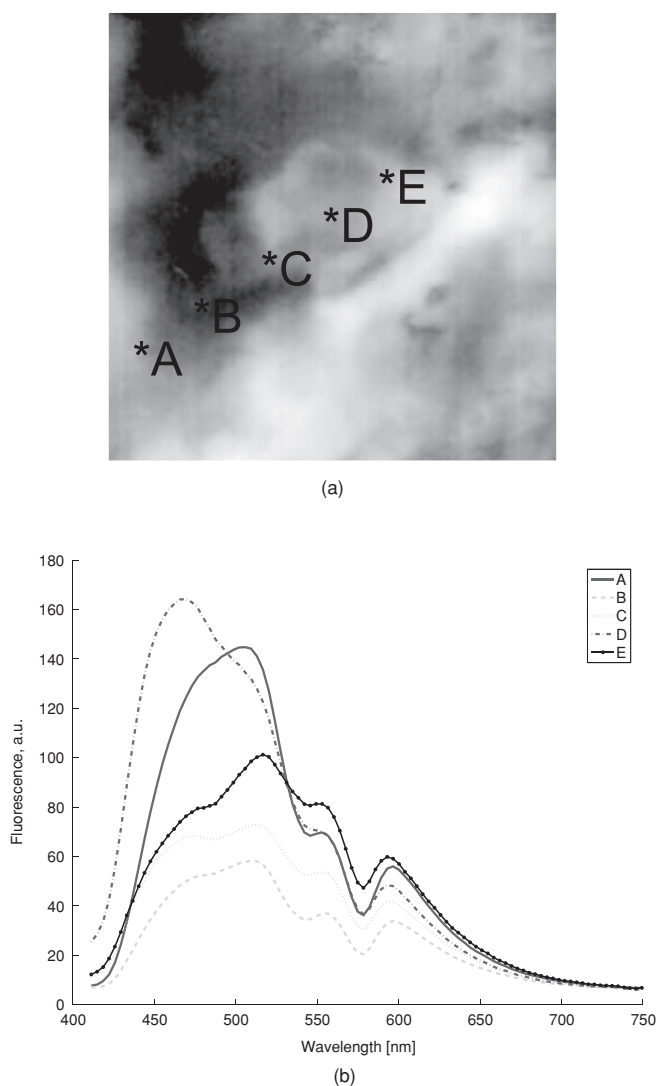
Fig. 10 (a) Atherosclerotic plaque under UV-excitation and (b) corresponding spectra.

(a)

(b)

Fig. 11 (a) PCA based on reflectance data and (b) PCA based on fluorescence data (normalized to peak intensity).

Jack-knife validation). The means of each group were not statistically different due to large standard deviation. Separate PCA analysis of the histology groups show that the groups were separable with respect to the first PCA component, but not to the second or third component, see Fig. 11. The mean of the PCA coefficients was found to be roughly independent on the contribution from individual samples. The largest intergroup variance was found in the grade IV-Va group.

5 Discussion

This study presents hyperspectral reflectance and fluorescence data of atherosclerotic plaques from human aortic samples, with focus on advanced lesions. Both white-light reflectance- and UV-excited fluorescence hyperspectral images were recorded. Plaques were analyzed and classified according to histology, and the recorded images were further analyzed by image analysis techniques.

Some spectral features shown in the apparent absorption spectra of Fig. 7(a) are similar to those found in the absorption spectra of hemoglobin, shown in Fig. 1. The most evident

is the absorption (around 414 to 418 nm) in the Soret-band and the characteristic peaks at 542 and 578 nm of oxygenated hemoglobin. The spectra of the grade VI-plaque differs significantly from the others as it has much higher apparent absorption, and also expresses low fluorescence as compared to the other grade lesions as shown in Fig. 7(b). This is largely due to the advanced pathological stage of the plaque with associated high blood content and large hemoglobin absorption due to hemorrhage. Hemoglobin absorption also efficiently quenches the fluorescence. Note also that the largest (Soret-band) absorption peak has red shifted to 433 nm as compared to 418 nm for the other spectra indicating deoxygenated hemoglobin, not to be unexpected in tissue *post mortem*. Previous work by our group have showed that methemoglobin was readily discernable in reflectance spectra if 20% of hemoglobin species were methemoglobin.[45] In the present work, no detectable amounts of methemoglobin were found, even in samples measured four days *post mortem*, probably due to the samples being kept hydrated and cool. The effect of cool storage conditions have been shown to preserve tissue with only minimal changes in the

optical properties up to 72 h *post mortem*; the largest changes related to deoxygenation of blood occurring only 5 to 10 min *post mortem*.[46]

Spectra from the other classification groups appear more homogeneous, and the local maximum in the 480 nm region is probably due to beta-carotene absorption, indicating the presence of lipids. The local minima of the fluorescent spectra for grade 0-I, Va and VI at 542 and 578 nm are also due to hemoglobin absorption. The same hemoglobin absorbance features are visible in spectra shown in Figs. 9 and 10 showing the reflectance and fluorescence spectra of an advanced lesion as one traverses the plaque from end to end. The signature on the spectra due to the presence of beta-carotene is also clearly visible. The spectrum of site E shows a large beta-carotene absorption in the 450 to 490 nm region, as a local maximum in absorption spectra shown in Fig. 9 and as a local minimum in fluorescence spectra in Fig. 10. This is coherent with the large number of superficial foam cells present as seen in histology. It is evident that plaque spectra, both reflectance- and fluorescence-, vary quite substantially with respect to the measurement site, again suggesting large plaque heterogeneity.

Principal component analysis was performed on averaged spectra (410 to 750 nm) extracted from *K*-means classification on noise-reduced images, only regarding the most central region of the plaques. A study of the variance of the PCA transformation found that the first three PCA-eigenvectors were significant. The most significant eigenvectors reveal that some absorption and fluorescence bands are prominent in both reflectance and fluorescence data. Extrema in the Soret-band and the 540 to 580 nm range are associated with oxy- and deoxyhemoglobin. Absorption peaks around 450 and 480 nm may be attributed to beta-carotene absorption. The by-far largest eigenvector peak based on fluorescence data was in the 480 to 490 nm range which is most probably due to collagen fluorescence. In addition, the effect of present absorbers such as oxy- and deoxyhemoglobin and beta-carotene was clearly visible in the eigenvectors from PCA of fluorescence spectra. It is thus important to have a wide spectral bandwidth to ensure that all relevant chromophores/fluorophores are detected, and avoid that the presence of undeclared components affect spectra, leading to misinterpretations of said spectra.

Our results show that calcified regions show the strongest overall fluorescence, while the lowest fluorescence can be observed from regions with high blood content and high beta-carotene absorption. Calcium is known to exhibit fluorescence upon 308 nm excitation[47] but does not fluoresce upon 335 nm,[48] and it is therefore not likely to fluoresce upon 355 nm excitation as used in the present study. The observed strong fluorescence may therefore be attributed to collagen/elastin covering the calcified regions, insulated from the quenching effect of hemoglobin and other strong absorbers. From the image analysis classification it was evident that the advanced lesions consist of a central region, enveloped by one or more regions with a slightly different spectral signature (Fig. 6). This was true for both white-light reflectance and fluorescence image data. Reconsidering the gross appearance of the samples, such surrounding regions often corresponded to the outer rim, or shoulder of the plaques. Regions outside of these plaques were of mostly normal wall composition (considering the age of subjects). It is evident that a single plaque may have regions of different characteristics, and

thus makes it hard to fit into the existing classification systems. However, since the plaques investigated in this study originated from the aorta, they are much larger than plaques found in the coronary arteries and may be more heterogeneous due to this fact alone.

The fluorescence data presented in this study are not corrected with respect to the background optical properties. This could have been done using an inverse optical transport model to derive the optical properties of the samples from the reflectance images, and then correcting the fluorescence data. However, complex and heterogeneous lesions are difficult to model accurately, and the contribution from the hemoglobin and beta-carotene absorption is considered to be an important feature of the individual plaque footprint. It was therefore chosen to use the normalized fluorescence and the calibrated reflectance data as input for the statistical image analysis. The effect of correcting the data with respect to background absorption will be tested in future work by modifying an existing photon transport model.[45]

The biopsies for histological examination were cut from the aorta samples using a scalpel, however the cutting imposed a practical problem as some pus and gruel fluids were squeezed out of the (advanced) plaques by the scalpel during cutting. This problem led to a disparity of the spectra recorded and the histology analyzed, which are hence not directly comparable due to different proportions of lipids. This effect is not pronounced if the lipids were deep within the tissue, however the origin of escaped lipids is uncertain as histology was also affected. Also, due to the unstable morphology of the plaques, the two plaques classified as grade VI by histology were disrupted (i.e., lost the top layer) during the fixation process. The recorded spectra, therefore, includes the cap-layer not present in histology.

Our current HSI-system is not an *in vivo* modality for detection of atherosclerotic plaques. However, HSI may still prove to be a candidate for a future modality identifying the vulnerable regions. This can be achieved by means of fiber-optic endoscopes, as demonstrated earlier in a HSI-system.[22] As with other optical modalities the presence of blood causes interference where even a thin layer can obscure underlying features.[49] This effect may, in an *in vivo* environment, be suppressed by saline flushing as commonly used in angioscopy. Optimized and automated image processing routines can provide a near real-time presentation of results. Invasive modalities always constitute a risk of complications, and even probe-based HSI may therefore not be suited as a screening tool. However, it may be useful in conjunction with other invasive interventions when they are medically required, e.g., percutaneous coronary intervention (PCI).

Regardless, the value of HSI-characterization *in vitro* may still reveal important information helpful for future modalities, even if HSI itself proves to be not optimally suited for *in vivo* characterization in a clinical setting. HSI may provide information which hopefully improves the current understanding of the vulnerability markers needed for a precise characterization of plaques, enabling a simpler future detection modality. This detailed spectral/spatial mapping capability means that HSI has a large potential in characterization of other tissues as well.

6 Conclusions

This paper has demonstrated the use of *in vitro* reflectance- and fluorescence hyperspectral imaging for the detection of

atherosclerotic plaques from aorta samples. Hyperspectral imaging and image analysis were shown to identify the complexity and large heterogeneity of such plaques as compared to histology. Most advanced lesions had a central region surrounded by an outer rim or shoulder-region of the plaque, which is considered a weak spot in vulnerable lesions. This spatial variation of plaques makes it hard to classify a plaque correctly, especially based on single-point spectroscopic measurements. This emphasizes the need to inspect the whole lesion to provide a more complete picture of the plaque pathology. Plaque features such as lipids and calcifications could be identified from white-light reflectance-, and UV-excited fluorescence hyperspectral images. Principal component analysis of spectra acquired from both reflectance and fluorescence HSI has shown that these provide both complementary information and some supplementary information of the lesions examined in this study. The influence of beta-carotene (indicating lipids) and oxy- and deoxyhemoglobin was apparent in both reflectance and fluorescence spectra, however some features indicating collagen is more apparent in fluorescence data.

The combination of spatial- and spectral information makes HSI a powerful tool for general tissue characterization, without the need of staining or sample preparation, and with a wide selection of established spectral-, statistical-, and powerful image-analysis tools available. Additional investigations will be carried out to develop the methodology further.

References

1. D. Lloyd-Jones, R. Adams, M. Carnethon, G. D. Simone, T. B. Ferguson, K. Flegal, E. Ford, K. Furie, A. Go, K. Greenlund, N. Haase, S. Hailpern, M. Ho, V. Howard, B. Kissela, S. Kittner, D. Lackland, L. Lisabeth, A. Marelli, M. McDermott, J. Meigs, D. Mozaffarian, G. Nichol, C. O'Donnell, V. Roger, W. Rosamond, R. Sacco, P. Sorlie, R. Stafford, J. Steinberger, T. Thom, S. Wasserthiel-Smoller, N. Wong, J. Wylie-Rosett, and Y. Hong, "Heart disease and stroke statistics—2009 update. A report from the American Heart Association statistics committee and stroke statistics subcommittee," *Circulation* **119**, e21–e181 (2009).
2. P. R. Moreno, R. A. Lodder, R. Purushothaman, W. E. Charash, W. N. O'Connor, and J. E. Muller, "Detection of lipid pool, thin fibrous cap, and inflammatory cells in human aortic atherosclerotic plaques by nearinfrared spectroscopy," *Circulation* **105**, 923–927 (2002).
3. M. B. Lilledahl, O. A. Haugen, M. Barkost, and L. O. Svaasand, "Reflection spectroscopy of atherosclerotic plaque," *J. Biomed. Opt.* **11**(2), 021005 (2006).
4. G. O. Angheloiu, J. T. Arendt, M. G. Müller, A. S. Haka, I. Georgakoudi, J. T. Motz, O. R. Scepanovic, B. D. Kuban, J. Myles, F. Miller, E. A. Podrez, M. Fitzmaurice, J. R. Kramer, and M. S. Feld,

5. C. Kittrell, R. L. Willett, C. de los Santos-Pacheo, N. B. Ratliff, J. R. Kramer, E. G. Malk, and M. S. Feld, "Diagnosis of fibrous arterial atherosclerosis using fluorescence," *Appl. Opt.* **24**(15), 2280–2281 (1985).
6. S. Andersson-Engels, J. Johansson, U. Stenram, K. Svanberg, and S. Svanberg, "Malignant tumor and atherosclerotic plaque diagnosis using laser-induced fluorescence," *IEEE J. Quantum Electron.* **26**(12), 2207–2217 (1990).
7. T. G. Papazoglou, "Malignancies and atherosclerotic plaque diagnosis: is laser induced fluorescence spectroscopy the ultimate solution," *J. Photochem. Photobiol. B* **28**, 3–11 (1995).
8. N. Anastassopoulou, B. Arapoglou, P. Demakakos, M. I. Makropoulou, A. Paphiti, and A. A. Serafetinides, "Spectroscopic characterisation of carotid atherosclerotic plaque by laser induced fluorescence," *Lasers Surg. Med.* **28**, 67–73 (2001).
9. M. E. Brezinski, G. J. Tearney, B. E. Bouma, J. A. Izatt, M. R. Hee, E. A. Swanson, J. F. Southern, and J. G. Fujimoto, "Optical coherence tomography for optical biopsy: properties and demonstration of vascular pathology," *Circulation* **93**, 1206–1213 (1996).
10. I.-K. Jang, G. J. Tearney, B. MacNeill, M. Takano, F. Moselewski, N. Iftima, M. Shishkov, S. Houser, H. T. Aretz, E. F. Halpern, and B. E. Bouma, "In vivo characterization of coronary atherosclerotic plaque by use of optical coherence tomography," *Circulation* **111**, 1551–1555 (2005).
11. C. T. Sherman, F. Litvack, W. Grundfest, M. Lee, A. Hickey, A. Chaux, R. Kass, C. Blanche, J. Matloff, L. Morgenstern, W. Ganz, H. J. C. Swan, and J. Forrester, "Coronary angioscopy in patients with unstable angina pectoris," *N. Engl. J. Med.* **315**, 913–919 (1986).
12. M. Asakura, Y. Ueda, O. Yamaguchi, T. Adachi, A. Hirayama, M. Hori, and K. Kodama, "Extensive development of vulnerable plaques as a pan-coronary process in patients with myocardial infarction: An angioscopic study," *J. Am. Coll. Cardiol.* **37**(5), 1284–1288 (2001).
13. P. D. Beule, D. M. Owen, H. B. Manning, C. B. Talbot, J. Requejo-Isidro, C. Dunsby, J. Mcginty, R. K. P. Benninger, D. S. Elson, I. Munro, M. J. Lever, P. Anand, M. A. A. Neil, and P. M. W. French, "Rapid hyperspectral fluorescence lifetime imaging," *Microsc. Res. Tech.* **70**(5), 481–484 (2007).
14. M. B. Lilledahl, O. A. Haugen, C. de Lange Davies, and L. O. Svaasand, "Characterization of vulnerable plaques by multiphoton microscopy," *J. Biomed. Opt.* **12**(4), 044005 (2007).
15. B. Khoobehi, J. M. Beach, and H. Kawano, "Hyperspectral imaging for measurement of oxygen saturation in the optic nerve head," *Inv. Opth. Vis. Sci.* **45**(5), 1464–1472 (2004).
16. W. R. Johnson, D. W. Wilson, W. Fink, M. Humayun, and G. Bearman, "Snapshot hyperspectral imaging in opthalmology," *J. Biomed. Opt.* **12**(1), 014036 (2007).
17. B. Farina, C. Bartoli, A. Bono, A. Colombo, M. Lualdi, G. Tragni, and R. Marchesini, "Multispectral imaging approach in the diagnosis of cutaneous melanoma: potentiality and limits," *Phys. Med. Biol.* **45**, 1243–1254 (2000).
18. L. L. Randeberg, I. Baarstad, T. Løke, P. Kaspersen, and L. O. Svaasand, "Hyperspectral imaging of bruised skin," *Proc. SPIE* **6078**, 60780O (2006).
19. G. N. Stamatas and N. Kollias, "In vivo documentation of cutaneous inflammation using spectral imaging," *J. Biomed. Opt.* **12**(5), 051603 (2007).
20. A. Vogel, V. V. Chernomordik, J. D. Riley, M. Hassan, F. Amyot, B. Dasgeb, S. G. Demos, R. Pursley, R. F. Little, R. Yarchoan, T. Tao, and A. H. Gandjbakhche, "Using noninvasive multispectral imaging to quantitatively assess tissue vasculature," *J. Biomed. Opt.* **12**(5), 051604 (2007).
21. D. G. Ferris, R. A. Lawhead, E. D. Dickman, N. Holtzapple, J. A. Miller, S. Grogan, S. Bambot, A. Agrawal, and M. L. Faupel, "Multimodal hyperspectral imaging for the noninvasive diagnosis of cervical neoplasia," *J. Low Genit. Tract. Dis.* **5**(2), 65–72 (2001).
22. M. E. Martin, M. B. Wabuyele, K. Chen, P. Kasili, M. Panjehpour, M. Phan, B. Overholt, G. Cunningham, D. Wilson, R. C. DeNovo, and T.

"Intrinsic fluorescence and diffuse reflectance spectroscopy identify superficial foam cells in coronary plaques prone to erosion," *Arterioscl. Throm. Vas.* **26**, 1594–1600 (2006).

Vo-Dinh, "Development of an hyperspectral imaging (hsi) system with applications for cancer detection," *Ann. Biomed. Eng.* **34**(6), 1061–1068 (2006).

23. B. S. Sorg, M. E. Hardee, N. Agarwal, B. J. Moeller, and M. W. Dewhirst, "Spectral imaging facilitates visualization and measurements of unstable and abnormal microvascular oxygen transport in tumors," *J. Biomed. Opt.* **13**(1), 014026 (2008).

24. A. M. Siddiqi, H. Li, F. Faruque, W. Williams, K. Lai, M. Hughson, S. Bigler, J. Beach, and W. Johnson, "Use of hyperspectral imaging to distinguish normal, precancerous, and cancerous cells," *Cancer Cytopathol.* **114**(1), 13–21 (2008).

25. M. E. Martin, M. B. Wabuyele, M. Panjehpour, M. N. Phan, B. F. Overholt, and T. Vo-Dinh, "Hyperspectral fluorescence imaging system for biomedical diagnostics," *Proc. SPIE* **6080**, 60800Q (2006).

26. G. Zavattini, S. Vecchi, G. Mitchell, U. Weisser, R. M. Leahy, B. J. Pichler, D. J. Smith, and S. R. Cherry, "A hyperspectral fluorescence system for 3d in vivo optical imaging," *Phys. Med. Biol.* **51**, 2029–2043 (2006).

27. M. E. Martin, M. Wabuyele, M. Panjehpour, B. Overholt, R. DeNovo, S. Kennel, G. Cunningham, and T. Vo-Dinh, "An AOTF-based dual-modality hyperspectral imaging system (DMHSI) capable of simultaneous fluorescence and reflectance imaging," *IEEE Eng. Med. Biol. Mag.* **28**(2), 149–155 (2006).

28. "The vulnerable atherosclerotic plaque: Understanding, identification, and modification," in *Clinical Photomedicine*, V. Fuster, Ed., Chap. 1, American Heart Association, Monograph Series, Futura Publishing Company, Inc., Armonk, NY (1998).

29. M. Naghavi, P. Libby, E. Falk, S. W. Casscells, S. Litovsky, J. Rumberger, J. J. Badimon, C. Stefanadis, P. Moreno, G. Pasterkamp, Z. Fayad, P. H. Stone, S. Waxman, P. Raggi, M. Madjid, A. Zarrabi, A. Burke, C. Yuan, P. J. Fitzgerald, D. S. Siscovick, C. L. de Korte, M. Aikawa, K. E. J. Airaksinen, G. Assmann, C. R. Becker, J. H. Chesebro, A. Farb, Z. S. Galis, C. Jackson, I.-K. Jang, W. Koenig, R. A. Lodder, K. March, J. Demirovic, M. Navab, S. G. Priori, M. D. Rekhter, R. Bahr, S. M. Grundy, R. Mehran, A. Colombo, E. Boerwinkle, C. Ballantyne, W. Insull, R. S. Schwartz, R. Vogel, P. W. Serruys, G. K. Hansson, D. P. Faxon, S. Kaul, H. Drexler, P. Greenland, J. E. Muller, R. Virmani, P. M. Ridker, D. P. Zipes, P. K. Shah, and J. T. Willerson, "From vulnerable plaque to vulnerable patient: A call for new definitions and risk assessment strategies, part I," *Circulation* **108**, 1664–1672 (2003).

30. H. C. Stary, A. B. Chandler, S. Glagov, J. R. Guyton, W. Insell Jr., M. E. Rosenfeld, S. A. Schaffer, C. J. Schwartz, W. D. Wagner, and R. W. Wissler, "A definition of initial, fatty streak, and intermediate lesions of atherosclerosis. A report from the committee on vascular lesions of the council on arteriosclerosis, American Heart Association," *Arterioscl. Throm. Vas.* **14**, 840–856 (1994).

31. H. C. Stary, A. B. Chandler, R. E. Dinsmore, V. Fuster, S. Glagov, W. Insull Jr., M. E. Rosenfeld, C. J. Schwartz, W. D. Wagner, and R. W. Wissler, "A definition of advanced types of atherosclerotic lesions and a histological classification of atherosclerosis. A report from the committee on vascular lesions of the council on arteriosclerosis, American Heart Association," *Circulation* **92**, 1355–1374 (1995).

32. R. Virmani, F. D. Kolodgie, A. P. Burke, A. Farb, and S. M. Schwartz, "Lessons from sudden coronary death. A comprehensive morphological

classification scheme for atherosclerotic lesions," *Arterioscl. Throm. Vas.* **20**, 1262–1275 (2000).

33. S. Prahl, "Optical absorption of Hemoglobin," Oregon Medical Laser Center, World Wide Web (1999). URL: http://omlc.ogi.edu/spectra/hemoglobin

34. W. G. Zijlstra, A. Buursma, and O. W. van Assendelft, *"Visible and near infrared absorption spectra of human and animal haemoglobin,"* VSP (2000).

35. N. Kollias, A. Baqer, I. Sdiq, and T. M. Sayre, "In vitro and in vivo ultraviolet-induced alterations of oxy- and deoxyhemoglobin," *Photochem. Photobiol.* **56**(2), 223–227 (1992).

36. D. H. Blankenhorn, D. G. Freiman, and H. C. Knowles, "Carotenoids in man: the distribution of epiphasic carotenoids in atherosclerotic lesions," *J. Clin. Invest.* **35**, 1243–1247 (1956).

37. H. Du, R.-C. A. Fuh, J. Li, L. A. Corkan, and J. S. Lindsey, "Photochemcad: A computer-aided design and research tool in photochemistry," *Photochem. Photobiol.* **68**(2), 141–142 (1998).

38. W. Stahl, U. Heinrich, H. Jungmann, J. von Laar, M. Schietzel, H. Sies, and H. Tronnier, "Increased dermal carotenoid levels assessed by noninvasive reflection spectrophotometry correlate with serum levels in women ingesting Betatene," *J. Nutr.* **128**(5), 903–907 (1998).

39. I. S. Saidi, S. L. Jacques, and F. K. Tittel, "Mie and rayleigh modelling of visible-light scattering in neonatal skin," *Appl. Opt.* **34**(31), 7410–7418 (1995).

40. L. I. Laifer, K. M. O'Brien, M. L. Stetz, G. R. Gindi, T. J. Garrand, and L. I. Deckelbaum, "Biochemical basis for the difference between normal and atherosclerotic arterial fluorescence," *Circulation* **80**, 1893–1901 (1989).

41. R. Richards-Kortum and E. Sevick-Muraca, "Quantitative optical spectroscopy for tissue diagnosis," *Annu. Rev. Phys. Chem.* **47**, 555–606 (1996).

42. T. Skauli, P. E. Goa, I. Baarstad, and T. Løke, "A compact combined hyperspectral and polarimetric imager," *Proc. SPIE* **6395**, 639505 (2006).

43. *ENVI User's Guide*, pp. 684–688, Research Systems Inc., ENVI version 4.2 August ed. (2005).

44. J. T. Tou and R. C. Gonzalez, *Pattern recognition principles*, Addison-Wesley Publishing Company, Reading, MA (1974).

45. L. L. Randeberg, J. H. Bonesrønning, M. Dalaker, J. S. Nelson, and L. O. Svaasand, "Methemoglobin formation during laser induced photothermolysis of vascular skin lesions," *Lasers Surg. Med.* **34**(5), 414–419 (2004).

46. E. Salomatina and A. N. Yaroslavsky, "Evaluation of the in vivo and ex vivo optical properties in a mouse ear model," *Phys. Med. Biol.* **53**, 2797–2807 (2008).

47. A. J. Morguet, B. Körber, B. Abel, H. Hippler, V. Wiegand, and H. Kreuzer, "Autofluorescence spectroscopy using a XeCl excimer laser system for simultaneous plaque ablation and fluorescence excitation," *Lasers Surg. Med.* **14**, 238–248 (1994).

48. L. Marcu, J. A. Jo, Q. Fang, T. Papaioannou, T. Reil, J.-H. Qiao, J. D. Baker, J. A. Freischlag, and M. C. Fishbein, "Detection of ruptureprone atherosclerotic plaques by time-resolved laser-induced fluorescence spectroscopy," *Ather.* **204**, 156–164 (2009).

49. M. B. Lilledahl, M. Barkost, M. W. Gran, O. A. Haugen, and L. O. Svaasand, "The effect of a thin bloodlayer on fluorescence spectroscopy," *Proc. SPIE* **6078**, 60782J (2006).